Supraglacial ponds regulate runoff from Himalayan debris-covered glaciers

Tristram D.L. Irvine-Fynn[1]*, Philip R. Porter[2], Ann V. Rowan[3], Duncan J. Quincey[4], Morgan J. Gibson[1], Jonathan W. Bridge[5], C. Scott Watson[4], Alun Hubbard[1,6], Neil F. Glasser[1]

[1]Centre for Glaciology, Department of Geography and Earth Sciences, Aberystwyth University, Aberystwyth, UK. [2]Department of Biological and Environmental Sciences, University of Hertfordshire, Hatfield, UK. [3]Department of Geography, University of Sheffield, Sheffield, UK. [4]School of Geography, University of Leeds, Leeds, UK.[5]Department of the Natural and Built Environment, Sheffield Hallam University, Sheffield, UK. [6]Centre for Arctic Gas Hydrate, Environment and Climate, Department of Geosciences, The Arctic University of Norway, Tromsø, Norway.

* Corresponding author: Tristram Irvine-Fynn (tdi@aber.ac.uk)

Key Points:

- The monsoon season runoff hydrograph from Khumbu Glacier displays progressive changes in diurnal timing and recession characteristics.
- We propose that observed hydrological behavior results from seasonal evolution of supraglacial ponds and connections.
- Predicted expansion of debris-covered areas and pond extents will influence downstream timing, availability and quality of meltwater in the Himalaya.

Abstract

Meltwater and runoff from glaciers in High Mountain Asia is a vital freshwater resource for one fifth of the Earth's population. Between 13% and 36% of the region's glacierized areas exhibit surface debris cover and associated supraglacial ponds whose hydrological buffering roles remain unconstrained. We present a high-resolution meltwater hydrograph from the extensively debris-covered Khumbu Glacier, Nepal, spanning a seven-month period in 2014. Supraglacial ponds and accompanying debris cover modulate proglacial discharge by acting as transient and evolving reservoirs. Diurnally, the supraglacial pond system may store >23% of observed mean daily discharge, with mean recession constants ranging from 31 to 108 hours. Given projections of increased debris-cover and supraglacial pond extent across High Mountain Asia, we conclude that runoff regimes may become progressively buffered by the presence of supraglacial reservoirs. Incorporation of these processes is critical to improve predictions of the region's freshwater resource availability and cascading environmental effects downstream.

1 Introduction

An estimated 1.4 billion people depend on freshwater sourced from snow and ice melt in High Mountain Asia [*Immerzeel et al*., 2010]. Although highly variable across the region, this meltwater typically contributes between 20% and 50% of the total annual runoff [*Bookhagen and Burbank*, 2010; *Immerzeel and Bierkens*, 2012; *Lutz et al*., 2014]. Contemporary observations [*Bolch et al*., 2012; *Kaab et al*., 2012; *Pritchard*, 2017; *Brun et al*., 2017] and predicted trends [e.g. *Shea et al*., 2015a; *Soncini et al*., 2016] of glaciers in the Himalaya demonstrate declining ice volumes, but highlight uncertainty over the associated glacio-hydrological impacts and consequent water stress arising from climate change. One important cause of this ambiguity is the presence of a supraglacial debris mantle present on many of the region's glaciers, which covers up to 36% of the glacierized area in the Everest region [*Bolch et al*., 2012; *Kaab et al*., 2012; *Scherler et al*., 2011; *Thakuri et al*., 2014]. This debris mantle commonly causes downglacier ablation areas to exhibit low surface gradients and velocities [e.g. *Quincey et al*. 2007; *Scherler et al*., 2011; *Thompson et al*., 2016; *Salerno et al*., 2017] and its overall extent is increasing and predicted to expand further [*Rowan et al*., 2015; *Thakuri et al*., 2014; *Bolch et al*., 2008]. Supraglacial debris exerts a critical influence on glacier response to climate forcing because, dependent on its thickness, debris can either accelerate or retard ablation [*Østrem* 1959; *Evatt et al.,* 2015]. This effect, coupled with the dynamic topography of the glacier surface, promotes highly heterogenous ablation and the formation of surface lakes and ponds, which are a common feature of receding debris-covered glaciers [*Reynolds*, 2000; *Benn et al*., 2012; *Gardelle et al*., 2011; *Watson et al*., 2016; *Bassnet et al*., 2013; *Miles et al*., 2016, 2017a,b; *Narama et al*., 2017]. However, the processes and causal relationships underpinning the spatial distribution of supraglacial ponds remain unclear [*Salerno et al*., 2017].

Supraglacial ponds are 'hotspots' of glacier ablation [*Mertes et al*., 2016] due to their reflective and thermal characteristics [*Sakai et al*., 2000; *Benn et al*., 2001; *Miles et al*., 2016; *Watson et al.,* 2017a] and the presence of bare-ice cliffs associated with pond formation and growth [*Sakai et al*., 2002; *Brun et al.,* 2016; *Watson et al*., 2017b]. Consequently, ponds may accelerate glacier thinning and recession and act as temporary meltwater storage reservoirs [*Benn et al*., 2001, 2012]. Ponds on debris-covered glaciers are commonly either transient features due to inception or collapse of near-surface or shallow englacial drainage routes and consequent drainage, or

appear 'perched' in closed basins where efficient flowpaths are absent [*Reynolds*, 2000; *Benn et al*., 2001; *Miles et al*., 2017b; *Watson et al*., 2017a]. Seasonally, ponds on Himalayan glaciers typically grow both in area and depth [*Watson et al.,* 2017a], attaining maximum extent mid-monsoon and declining in size thereafter [*Miles et al*., 2017a; *Narama et al*., 2017; *Watson et al*., 2016]. Inter-annually, debris redistribution and change in surface topography results in variation in pond positions [*Narama et al*., 2017; *Watson et al*., 2016] and as ponds attain their local hydrological base-level they may evolve into larger scale lakes [*Thompson et al*., 2016; *Mertes et al*., 2016]. Observations of supraglacial pond water quality confirm that hydrological linkages do exist between ponds [*Takeuchi et al*., 2000; *Bhatt et al*., 2016], and pond extent may be governed by the evolving development and (re)organization of supraglacial drainage systems [*Watson et al*., 2016, 2017a; *Miles et al.,* 2017b]. Yet the extent to which these ponds impact upon meltwater generation and modify the seasonal hydrograph remains poorly quantified.

A lack of *in situ* observations of meltwater generation, transit and runoff for Himalayan glaciers [*Immerzeel et al*., 2012; *Bajracharya et al*., 2015] has led to uncertainties in the prediction of their hydrological response to environmental forcing. For example, some numerical models of debris-covered glacier systems utilize a linear reservoir parameterization linking proglacial discharge to meltwater production [e.g. *Ragettli et al*., 2015; *Fujita and Sakai*, 2014]. Such methods though fail to account for the potential hydrological complexities in the region. Specifically, the presence of interconnected supraglacial ponds implies a potentially complex hydrological system [*Miles et al.*, 2017b] that will modulate the water inputs to, and outputs from the glacier system. Hence, the acquisition of detailed measurements characterizing the hydrological behavior of debris-covered glaciers on diurnal to seasonal timescales is an imperative for improved predictions of meltwater delivery to downstream water resources throughout the Himalaya. Here, we present the results of a glacier-scale runoff monitoring program at the debris-covered Khumbu Glacier in the Everest region of Nepal. Our measurements span a 190-day period from April to November 2014 including the summer monsoon season.

2 Field Site and Methods

Khumbu Glacier (27.97°N, 86.83°E) flows from the southern flanks of Mount Everest to its terminus at ~4900 m a.s.l. (Figure 1a). The terminus elevation is slightly lower than the local

74 permafrost limit of ~5000 m a.s.l. [*Schmid et al.,* 2015]. The glacier is likely to be polythermal,
75 with an estimated 17 m deep cold surface ice layer [*Mae et al.*, 1975]. The glacier thinned at
76 approximately –0.6 m a^{-1} between 2000 and 2015, with losses of –1.4 m a^{-1} at elevations of
77 5200–5300 m [*King et al.,* 2017]. Approximately 47% of the 41 km^2 glacier including the
78 Changri Nup and Changri Shar tributaries is debris-covered (Figure 1b). Supraglacial debris
79 thickness varies from 0.1 m to over 3 m and is concentrated over the lowermost 8 km of the
80 glacier [*Soncini et al*., 2016], overlying 20 m to 440 m of glacier ice [*Gades et al*., 2000]. Recent
81 observations [e.g. *Nuimura et al*., 2011] indicate that this debris cover has become increasingly
82 topographically uneven: differential ablation has resulted in a complex glacier surface
83 characterized by the presence of numerous supraglacial water bodies [*Wessels et al*., 2002;
84 *Watson et al*., 2016]. Throughout 2014, ~1% of the total debris-covered area comprised
85 supraglacial ponds (Figures 1b-e). However, as elsewhere in the region, the hydrological
86 evolution and connectivity of these supraglacial ponds is poorly constrained. The Changri Nup
87 and Changri Shar tributaries are now physically disconnected, but retain a surface hydrological
88 connection with the Khumbu Glacier tongue [*Vincent et al*., 2016]. The only visible source of
89 meltwater runoff flowing from the Khumbu catchment emerges from a turbid supraglacial lake
90 situated close to the eastern glacier margin (Figure 1c). There is no evidence of alternative,
91 active terminal or lateral outlets for englacial or subglacial drainage pathways. Runoff data were
92 recorded immediately downstream of this outlet lake, where meltwater drains via a breach in the
93 eastern Little Ice Age lateral moraine to the upper Dudh Koshi.

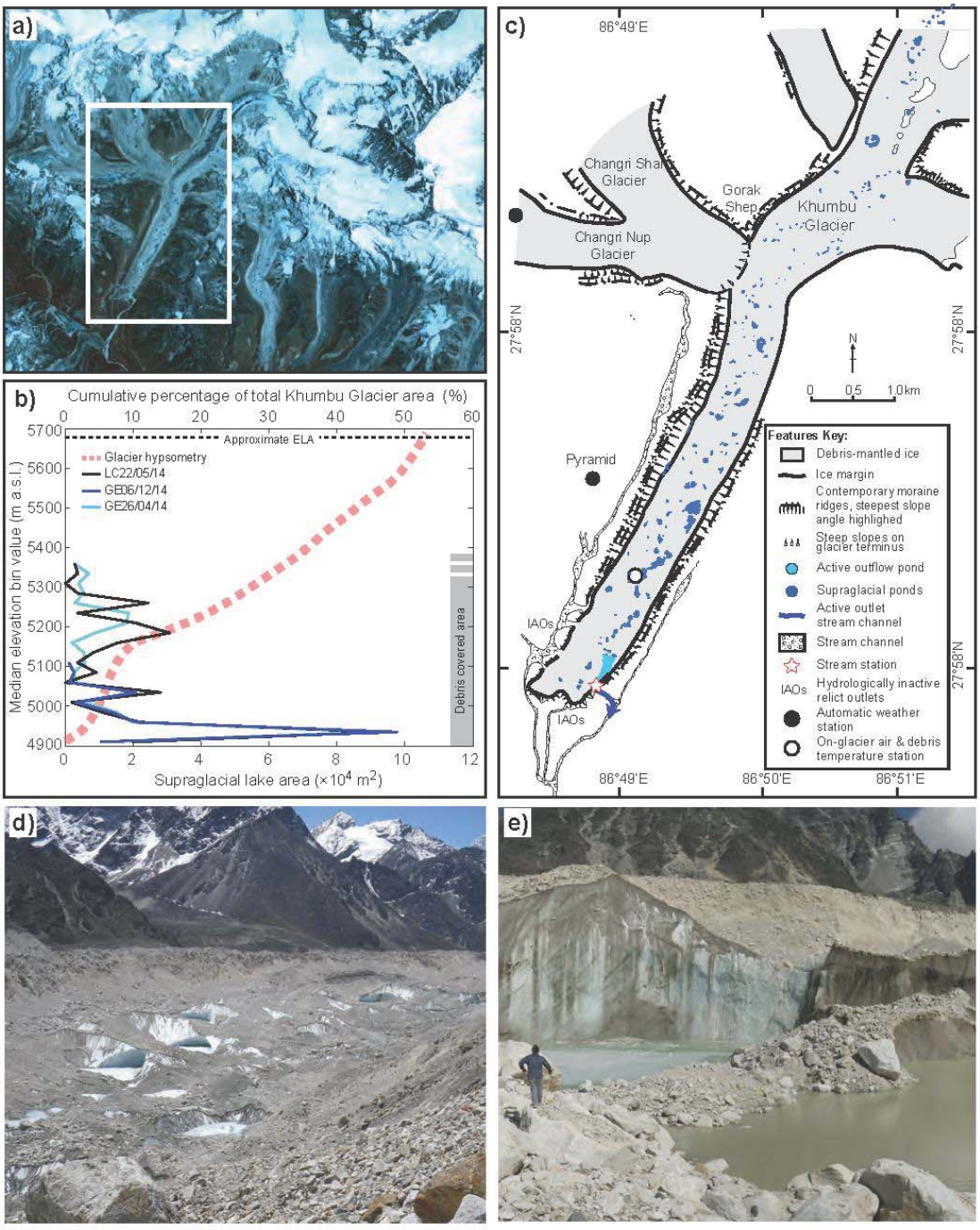
a)
b)
Cumulative percentage of total Khumbu Glacier area (%)
0
10
20
30
40
50
60
Approximate ELA
Glacier hypsometry
LC22/05/14
GE06/12/14
GE26/04/14
Median elevation bin value (m a.s.l.)
5700
5600
5500
5400
5300
5200
5100
5000
4900
Debris covered area
0
2
4
6
8
10
12
Supraglacial lake area (×10^4 m^2)
c)
86°49'E
Changri Shar Glacier
Changri Nup Glacier
Gorak Shep
Khumbu Glacier
27°58'N
N
0
0.5
1.0km
Pyramid
IAOs
IAOs
IAOs
Features Key:
Debris-mantled ice
Ice margin
Contemporary moraine ridges, steepest slope angle highlighed
Steep slopes on glacier terminus
Active outflow pond
Supraglacial ponds
Active outlet stream channel
Stream channel
Stream station
Hydrologically inactive relict outlets
Automatic weather station
On-glacier air & debris temperature station
86°49'E
86°50'E
86°51'E
d)
e)

Figure 1: (a) ASTER imagery (Sept 2012) of the Everest region, Nepal, outlining lower elevations of the Khumbu Glacier detailed in (c); (b) hypsometry and supraglacial pond area in Khumbu Glacier ablation zone based on satellite imagery from 26 April, 22 May and 6 December 2014 [see *Watson et al*., 2016]; (c) ablation zone of Khumbu Glacier highlighting key data collection sites and major geomorphological features, including hydrologically inactive outlets (IAOs) indicative of abandoned drainage routes and supraglacial lake positions on 26 April 2014 prior to the onset of the monsoon season; (d, e) oblique images illustrating typical debris cover and pond morphology, taken during the pre-monsoon period, May 2014.

Discharge (Q) data were collected between 14 May and 12 November (Day of Year (DOY) 135 to 317) using standard methods [*Herchy*, 1995]. A hydrological monitoring station was established in a stable reach of the sole outflow channel at 4930 m a.s.l.. Average water stage was recorded at 30 min intervals using a Druck PDCR1730 pressure transducer and Campbell Scientific (CS) CR1000 data logger. A stage-discharge rating curve was developed using triplicate dilutions [*Hudson and Fraser*, 2005] of 3 mL aliquots of 10% fluorescein and a Turner Designs Cyclops7 fluorometer linked to a CS CR10X datalogger. A non-linear stage-discharge relationship yielded a coefficient of determination of $r^2 = 0.79$ ($n = 18$). Estimated uncertainty in Q is <15%, although this is increased for higher Q values [see *Supplementary Information*; *Rantz et al*., 1982; *Sakai et al*., 1997; *DiBaldassarre and Montanari*, 2009]. On-glacier air temperature (T_a) and debris temperature (T_d) were monitored at 4935 m a.s.l. using Gemini TinyTag2 logging thermistors with a stated measurement accuracy of ±0.4°C (Figure 1c). The T_a sensor was mounted in a naturally aspirated radiation shield 1 m above the debris surface; the T_d sensors were located within the debris layer at depths of 0.55 and 1.0 m below the surface and away from the debris-ice interface. All temperature measurements were recorded at 30-min intervals. Local incident shortwave radiation (SW_{in}) was recorded at an automatic weather station 5363 m a.s.l. on the Changri Nup Glacier (Figure 1c) using a Kipp & Zonen CNR4 sensor with 3% uncertainty. Precipitation (P) was measured at Pyramid Observatory (Figure 1c) at 5035 m a.s.l. using a Geonor T-200 gauge; these hourly data were corrected for undercatch of solid precipitation and have an estimated accuracy of ±15% [*Sherpa et al.*, 2017].

We examined the timing of peak discharge and the shape of the diurnal hydrograph using standard approaches; lag times between time-series were identified using a moving window cross-correlation [e.g. *Jobard and Dzikowski*, 2006], while we classified diurnal hydrographs using a paired Principal Components Analysis (PCA) and Hierarchical Cluster Analysis (HCA) approach [e.g. *Hannah et al*., 2000; *Swift et al*., 2005]. Specifically, daily (24 hr) hydrographs were assumed to commence at low Q at 06:00, PCA was conducted without rotation and only components with eigenvalues > 1.0 were retained. PCA identified modes of diurnal Q variation defined by the standardized component loadings and these loadings for each day were clustered using Euclidean distance measures and a within-groups linkage method. A total of 6 groups were identified and further classified using a second, independent HCA that defined diurnal hydrograph similarity based on key discharge metrics following z-score normalization. Daily hydrographs were then described based on 'shape' defined by PCA clusters and 'magnitude' identified in the secondary HCA.

Estimates of recession storage constants (K) for each diurnal hydrograph were derived from semi-logarithmic plots of Q versus time [e.g. *Gurnell*, 1993; *Hodgkins et al*., 2013] where:

$$\mathbf{K} = \frac{-t}{ln\left(\frac{Q_t}{Q_0}\right)} \qquad \text{Eq.1}$$

for which t is time since the start of the recession segment, and Q_0 and Q_t the discharge at the start of the recession segment and at time t, respectively. For all days classified as exhibiting diurnal discharge cycles (n = 117) or constant recessional hydrographs (n = 29), K-values were calculated from the time-step following peak discharge, or from 18:00 in the case of persistent recession hydrographs. Recession segments and associated aggregate recession constants were identified using segmented linear regression for cases exhibiting durations >1 hr.

3 Results

The meteorological and discharge time-series (Figure 2a-d) for the 2014 monsoon season reveal that T_a and SW_{in} exhibited strong diurnal variations, with highest incident energy fluxes between 10:00 and 15:00, as typifies the region [see *Shea et al*., 2015b]. These two variables were highly correlated over the diurnal cycle ($r > 0.5$, $p < 0.05$) throughout the observation period (Figure

2e). Seasonal changes in T_d aligned well with T_a, although at the daily timestep, correlation suggested a changing lag between variables (Figure 2e). Despite a distinct diurnal variability in T_d, variation was suppressed at depth (Figure 2b), and T_d remained below 0°C following DOY 300. The seasonal pattern of Q broadly followed that of T_a with an underlying diurnal fluctuation of between 0.005 and 12.3 $m^3 s^{-1}$, and daily mean Q peaking at ~9 $m^3 s^{-1}$ which compares well with published records of discharge during 2014 for the upper Dudh Koshi [*Soncini et al*., 2016; see *Supplementary Information*]. Interestingly, diurnal correlation indicated Q and both T_a and SW_{in} vary out of phase for much of the observation period (Figure 2e). Q lagged T_a progressively decreasing from 12 to 6 hrs until DOY 220, and subsequently returning to lags >12 hrs until DOY 285 when lags dropped again to ~6 hrs (Figure 2f). The diurnal hydrograph cycle became steadily delayed until DOY270 when T_d declined to ~5°C and continued to fall when a protracted hydrograph recession dominated. While statistically significant diurnal correlations between Q and P were found, these were inconsistent and showed no systematic trend (Figure 2e). Lag analysis highlighted statistically significant correlations ($r > 0.405$, $p < 0.05$) between Q and P over 24 hr periods, predominantly with Q lagged by >10 hrs, however no pattern in lag time was observed.

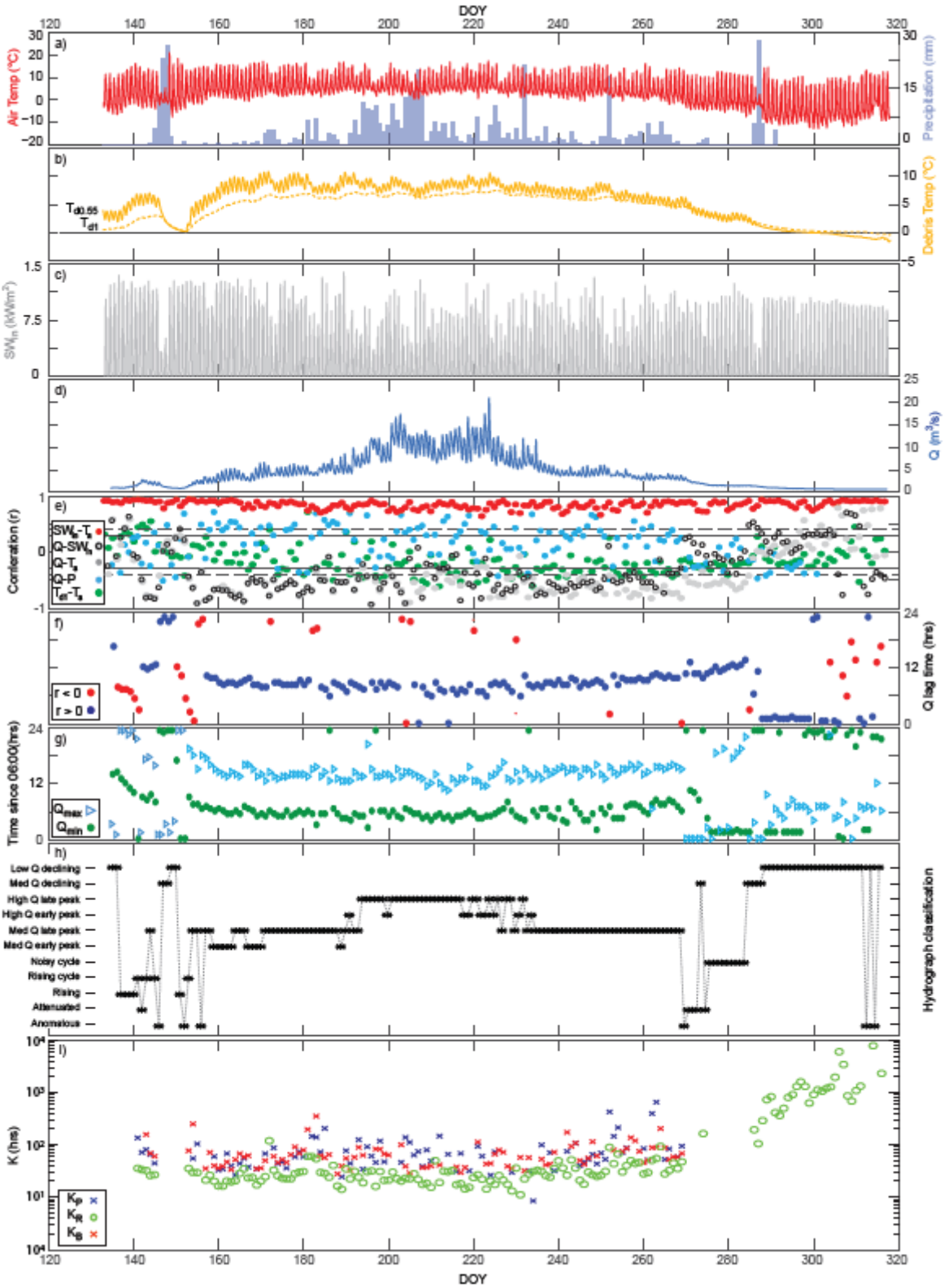
DOY
a)
Air Temp (°C)
Precipitation (mm)
b)
$T_{d0.55}$
T_{d1}
Debris Temp (°C)
c)
SW_{in} (kW/m²)
d)
Q (m³/s)
e)
Correlation (r)
SW_{in}-T_a
Q-SW_{in}
Q-T_a
Q-P
T_{d1}-T_a
f)
r < 0
r > 0
Q lag time (hrs)
g)
Time since 06:00(hrs)
Q_{max}
Q_{min}
h)
Low Q declining
Med Q declining
High Q late peak
High Q early peak
Med Q late peak
Med Q early peak
Noisy cycle
Rising cycle
Rising
Attenuated
Anomalous
Hydrograph classification
i)
K (hrs)
K_P
K_R
K_B
DOY

166

Figure 2: Time-series of (a) on-glacier air temperature T_a and total daily precipitation P, (b) debris temperature T_d at 0.55 and 1.0 m below the debris surface, (c) incident shortwave radiation SW_{in} and (d) meltwater discharge Q. Analyses identify (e) daily correlations between T_a, SW_{in}, P and Q with the 95% confidence levels indicated for the hourly ($r \approx 0.41$) and half-hourly ($r \approx 0.29$) data sets, (f) the lag time between daily peak T_a and maximum Q, (g) the timing of minimum and maximum Q, (h) the daily hydrograph classification based on shape and magnitude, and (i) the three principal hydrograph recession constants (K_P, K_R and K_B).

Three sequential recession segments were identified as typical within the time-series: (i) slow decrease in Q lasting $\leq$ 7 hours immediately following peak Q (K_P), (ii) major recession component of rapid decrease in Q over ~9 hours duration (K_R), and (iii) a second slow decrease for ~5 hours prior to the onset of the next diurnal cycle (K_B). Where only a singular extended recession was identified, this was taken to be K_R. K_P and K_B were found to be statistically similar, but lacked a significant temporal trend, while K_R showed a strong non-linear association with peak Q, decreasing and increasing as the monsoon season progressed. While aggregate K-values broadly agree with the magnitude of those identified in other glacial runoff records (mean K_P = 86.7 and K_B = 72.4 hrs, while mean K_R = 108 hrs for the season, but 31.1 hrs before DOY270), the recession segment pattern contrasts with the commonly reported systematic increase in K-values over diurnal hydrograph recession segments [e.g. *Gurnell*, 1993; *Hodgkins et al.*, 2013]. No association between K-values and P or daily peak Q was found. In tests, uncertainty related to the rating curve used to derive the Q time-series [see *Supplementary Information*; *Rantz et al.*, 1982] did not impact the recession patterns identified; however, if using a power-law rating curve [*Herchy*, 1995], recession constants K_P, K_R and K_B increased by 81±30%, 51±50% and 57±26% respectively.

4 Discussion

Our results from Khumbu Glacier indicate a hydrological configuration with both similarities and distinct differences to those typically reported for Alpine glacier systems in Europe and

elsewhere. Systematic progression in timing of peak Q, seasonal undulation in diurnal discharge amplitude, diurnal hydrograph asymmetry, and clear patterns in hydrograph classification are commonly described for temperate, debris-free alpine glaciers [e.g. *Richards et al*., 1996; *Hannah et al.*, 2000; *Swift et al*., 2005; *Jobard and Dzikowski*, 2006]. Typically, as the snowline recedes upglacier and melt season advances, peak Q occurs progressively closer to the time of heightened SW_{in} and T_a and, even for large south-facing valley glaciers such as Aletschgletscher, equivalent in size to Khumbu Glacier, Q lags the meteorological drivers of melt by <5 hrs during much of the ablation season [e.g. *Lang*, 1973; *Verbunt et al*., 2003]. As ablation continues on debris-free glaciers, the amplitude of Q increases, and the hydrograph form becomes more accentuated. Here, particularly prior to DOY230 (Figures 3f-h), the patterns of hydrograph characteristics resemble those reported for temperate alpine settings.

However, in contrast to debris-free alpine counterparts, the timing of daily peak and minimum discharge at Khumbu Glacier shows a more marked delay relative to meteorological drivers of ablation: peak Q occurs ≥6 hours after maximum SW_{in} and T_a, while minimum Q commonly coincides with peak irradiance. Q lagging energy fluxes reflects the delay in energy transfers that initiate melt, particularly for those associated with exchange at the atmosphere-debris interface and through the debris layer [*Carenzo et al*., 2016] (Figure 2b). Further lags may relate to meltwater transit to the monitoring site. Transition in lag time between T_a and Q mid-season is ascribed to changes in weather systems and lapse rates reported for the region during the monsoon [e.g. *Shea et al*., 2015b, *Steiner and Pelliciotti* 2016], the reduction in both T_a and SW_{in}, and subtle changes in the hydrological function of the drainage system. The lack of association between Q and precipitation has been observed elsewhere on debris-covered glaciers [e.g. *Thayyen et al*., 2005]. However, the elongated diurnal hydrograph recession diverges notably from other glacial observations and more specifically recession data reported here evidence neither ‘fast’ supraglacial and ‘moderate’ en- and sub-glacial drainage flowpaths, superimposed on a ‘slow’ persistent baseflow on a diurnal basis, nor a seasonal decline in recession storage constants [cf. *Gurnell*, 1993]. Furthermore, the gauging station elevation (4930 m a.s.l.), ensures the Q record solely relates to the supraglacial (debris-covered) and shallow englacial environment. Observations during 2014 confirmed that some supraglacial meltwaters entered a shallow englacial network, potentially allowing flow between supraglacial ponds, evidenced by spatial variability in pond turbidity which suggested hydrological connectivity

(Figure 1e) [see *Takeuchi et al*., 2012]. While geomorphic signatures suggested that meltwater that had once drained or followed seepage pathways through other moraine breach locations, contemporary field observations indicate these are relict inactive features (IAOs: Fig. 1c). Consequently, we discuss our data in the context of a conceptual model of the dominantly supraglacial drainage system illustrated in Figure 3, comprising a debris layer punctuated by a cascade of lakes or ponds.

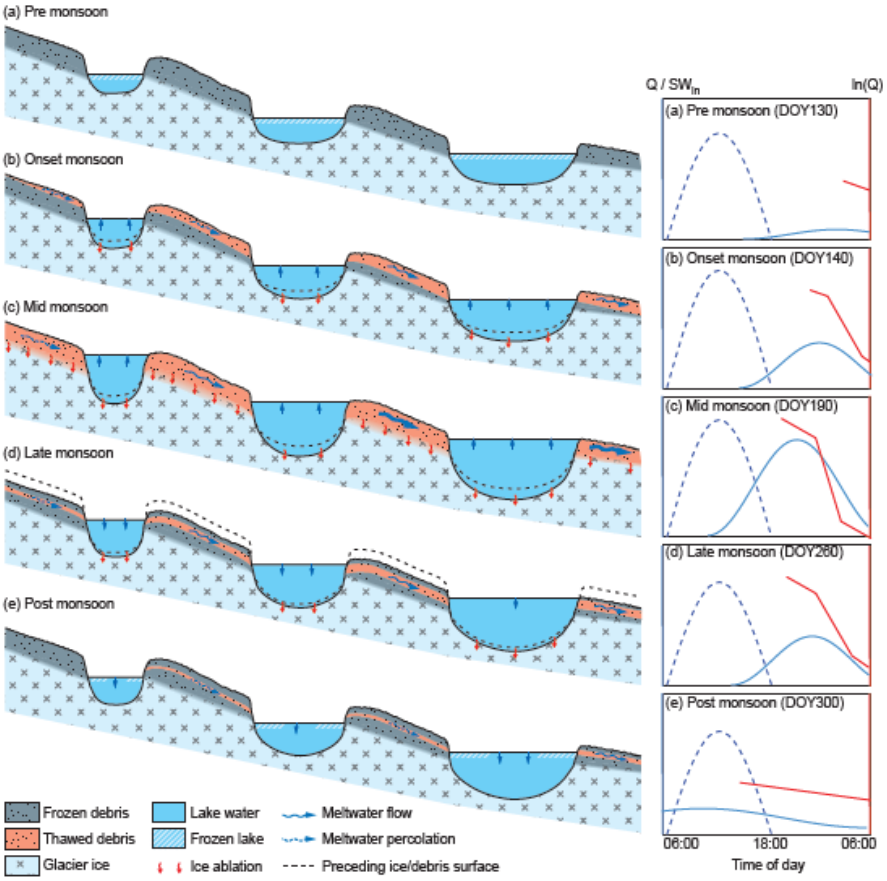

Figure 3: Conceptual model of the seasonal hydrological development of the surface of a Himalayan debris-covered glacier over an annual cycle. Indicative daily hydrometeorological plots for each stage are shown with SW_{in} (dashed), Q (blue), and a natural logarithmic transformed Q used to identify the recession components (red). Pre-monsoon (a) the surface is frozen following the winter period, but as the monsoon season approaches (b), the debris-cover begins to thaw, and water derived from melting intra-clast ice and ponds commences flow and thermal ablation at the base of ponds. Mid monsoon (c) the debris is fully thawed, ponds become connected and glacier ice melt occurs and ponds deepen through thermal ablation, which, coupled with monsoon rainfall, leads to more efficient drainage over the glacier ice surface. Towards the end of the monsoon season (d) the air temperatures drop and initiate freezing at the debris surface, while reductions in water flow facilitate upward freezing at the base of the debris layer; however, the thawed portion of the debris layer still transfers meltwater from ponds towards the glacier margin, albeit delayed. Post monsoon (e), which aligns with the latter portion

of our records, continued freeze-up of the lake and debris layer occurs restricting any transmission of meltwater as winter approaches and the glacier-wide hydrological system drains.

The cascade of developing ponds represents a series of reservoirs capable of temporarily storing meltwater and delaying its transit downstream. Combining the pre-monsoon pond areas (~ 2.5×10^5 m^2; Figure 1) with observation of the outflow lake level varying by ~0.7 m over a diurnal melt cycle, we estimate the supraglacial pond cascade on Khumbu Glacier to account for a minimum daily storage capacity of ~1.75×10^5 m^3 (equivalent to 23% of the observed mean daily discharge). Supported by evidence of progressive pond deepening during the monsoon season [e.g. *Watson et al*., 2017a] we conclude that the diurnal storage capacity of the pond system alone, not including the porous debris layer, can readily accommodate the observed daily mean P (~1.23×10^5 m^3 over the whole glacier area). The timing and magnitude of on-glacier storage may also be controlled by freeze-thaw processes, analogous to a periglacial environment given the local permafrost limit. During the winter, both the supraglacial debris layer and ponds are largely frozen, likely becoming impermeable and unable to convey any surface meltwater. As the monsoon season develops, the system progressively thaws [e.g. *Sakai et al*., 2000; *Benn et al*., 2001; *Namara et al*., 2017; *Miles et al*., 2016; *Watson et al*., 2017a]. The ponds may become hydrologically linked by three key flowpaths: those within the debris-covered mantle; shallow debris-filled crevasses [e.g. *Benn et al*., 2012; *Gulley and Benn*, 2007] or channels formed from collapsed near-surface englacial conduits [*Miles et al*., 2017b]; or debris- or water-choked near-surface passages [*Watson et al*., 2017a]. Published figures for heterogeneous debris indicate permeability of between 10^{-2} to 10^{-6} m s^{-1} [*Parriaux and Nicoud*, 1990; *Muir et al*., 2011; *Woo and Steer*, 1983; *Gulley and Benn*, 2007] although mobilization of fines may further reduce hydraulic efficiency [*Woo and Xia*, 1995]. When thawed, therefore, we anticipate the debris layer and associated supraglacial and shallow or collapsed englacial features may act as a depth-limited, transient storage reservoir, regulating bulk meltwater discharge over the glacier surface and between ponds and hence moderating the overall diurnal flow variance. The debris layer is underlain by glacier ice with discrete, spatially limited, shallow englacial flowpaths analogous to continuous permafrost with isolated, closed talik. The result, in the monsoon-influenced climate, is a thermal regime dominated by the seasonal freezing and thawing of the debris layer, as is

evident in our T_d time-series, and for which the correlations between T_a and T_d (Figure 2e) likely reflect change in debris heat capacity with water content. Khumbu Glacier's supraglacial debris layer may therefore be considered equivalent to a seasonally cryotic active layer [*Bonnaventure and Lamoureux*, 2013].

As the monsoon season progresses, evolution of the debris mantle hydrological system may result in increased inter-pond connectivity. Progressive thaw at depth in the debris layer and glacier ice melt, despite enlarging the supraglacial storage capacity, also aids the development of increasingly efficient supra-permafrost drainage: inter-clast ice is replaced with water flow pathways and increased hydraulic permeability [*Woo and Steer*, 1983; *Woo and Xia*, 1995], providing more efficient connections through the debris and facilitating debris-ice interface and englacial flowpath development [*Gulley and Benn*, 2007; *Gulley et al*., 2009; *Miles et al*., 2017b; *Watson et al*., 2017a]. Strengthening connectivity increases the rapidity of runoff through the cascading pond system. Sporadic activation, modification or abandonment of flowpaths and diurnal or seasonal variation in supraglacial pond storage capacity likely contributes to the observed variation of discharge recession (Fig. 3i). Such delay, peak flow suppression and attenuated recession, as seen in our data, are indicative of level-pool routing controlling meltwater transfer through a series of reservoirs [*Montaldo et al*., 2004] and, as such, the ponds may be conceptualized as thermokarst [*Kirkbride*, 1993].

Evidence for this role of supraglacial ponds and debris as regulators of meltwater discharge is exemplified by the diurnal hydrograph recession. When pond levels are at their peak or minima at seasonal and diurnal time-scales, K_P and K_B are determined by the hydraulic conductivity of the (thawed) debris that separates the individual pond basins. K_P was not clearly associated with either T_a or SW_{in} nor with daily maximum discharge; the recession segment was not associated with the magnitude of meltwater production. Once daily meltwater provision declines or ceases, changes in hydraulic head drive drainage through the pond cascade and the major recession (K_R) is governed by outflow channel geometry rather than rates of inflow controlled by debris permeability. K_R remains broadly consistent over the hydrologically active period (DOY134-270). Subsequently, particularly as T_a and T_d both fall and water drains from the pond cascade, water within the debris layer and debris-rich hydraulic connections between ponds refreezes, and

304 the hydraulic efficiency of the system declines. This change is highlighted by $K_R > K_B$, the post-
305 monsoon increase in K_R and a strongly negative, non-linear relationship between K_R and peak Q.

306 The observations following DOY 230 of declining Q despite positive T_a and T_d and precipitation
307 contributions are counterintuitive. However, given our hydrological analysis and conceptual
308 model it seems reasonable to suggest that this effect could have arisen from the fully thawed
309 debris layer readily storing excess water produced in this period and mobilization of fines
310 impinging on hydrological efficacy, with a consequent net reduction in throughflow evidenced
311 by gradual increases in all K-values. The drainage of meltwater continued for ~45 days after
312 night time T_a dropped to freezing, with around 7% of the observed runoff volume being
313 delivered in this late- and post-monsoon period. This protracted drainage corresponds well to the
314 delay in runoff thought to relate to hysteresis caused by a deep groundwater system in the Nepal
315 Himalaya [*Andermann et al*., 2012]. Our data suggest that widespread supraglacial debris layers
316 themselves may contribute to the observations of reservoir behavior in glacierized catchments at
317 a seasonal timescale, and extend the duration of glacier meltwater delivery to downstream
318 environments.

319 **5 Conclusions**

320 We have demonstrated that the evolving system of supraglacial ponds and accompanying debris
321 has the capacity to act as a fundamental modulator of proglacial discharge regimes at Khumbu
322 Glacier. Although there is uncertainty in the causal associations between glacier surface gradient,
323 debris cover and pond occurrence [*Salerno et al*., 2017], supraglacial ponds are reported to be
324 increasingly prevalent on debris-covered glaciers and represent an active and dynamic
325 hydrological system [*Miles et al*., 2017a,b; *Narama et al*., 2017; *Watson et al*., 2016, 2017a].
326 Recently, there has been growing recognition that small changes in hydrological function in
327 mountain regions can have substantial impacts on freshwater availability [e.g. *Pritchard*, 2017]
328 and biodiversity [*Jacobsen et al*., 2012] in terrestrial water bodies and ecosystems in the
329 Himalaya [*Xu et al*., 2009; *Salerno et al*., 2016]. To understand the hydrological response of
330 debris-covered glaciers and to forecast changes in water resources and ecosystem services in the
331 region, it is crucial to explicitly incorporate processes relating to the thermodynamics and
332 hydrology of widespread debris mantles that can now be considered as cryotic, thermokarstic
333 active layers – systems that are more commonly described solely in periglacial settings

[*Bonnaventure and Lamoureux*, 2013]. Further geophysical and hydrochemical exploration of debris cover [e.g. *Muir et al*., 2011; *McCarthy et al*., 2017] is needed to better define the nature of the supraglacial debris-covered drainage system and the modes and thermodynamics of hydraulic connectivity between ponds. With ~75 to 90% glacier area in the Himalaya above 4500–5000 m a.s.l., the elevation range commonly associated with the regional permafrost limit [*Schmidt et al*., 2015], processes we describe here should be widely applicable throughout the region and highlight the important role that debris-layer supraglacial hydrology may have on mediating glacier runoff characteristics in High Mountain Asia. Long-term increases in areal extent of debris cover and ponds will not only contribute to more rapid glacier mass loss but, we propose, also alter patterns of meltwater supply and quality to downstream catchments through their roles as temporary reservoirs and flow regulators. A more complete understanding of this buffering process is crucial to improving projections of the region's future water resources in a changing climate.

Acknowledgments and Data

All authors acknowledge the Royal Society (Research Grant: RG120393) and the British Society for Geomorphology. Summit Treks provided logistical support in Nepal. Patrick Wagnon kindly provided incident radiation and precipitation data. TDI, PRP, NFG and JWB led the analysis, writing and conceptual development. TDI, AVR, DJQ and MJG undertook fieldwork in Nepal. PRP provided fieldwork equipment and instruments. CSW acquired and processed supraglacial lake data. All authors contributed to development, editing and revision of the final manuscript. We thank the two reviewers who both provided insightful suggestions to help improve the paper.

All new data presented here are available via www.pangaea.de :
doi.org/10.1594/PANGAEA.883071 and doi.org/XXXXXXX

References

Andermann, C., L. Longuevergne, S. Bonnet, A. Crave, P. Davy and R. Gloaguen (2012). Impact of transient groundwater storage on the discharge of Himalayan rivers. *Nature Geoscience*, 5, 127-132.

Bajracharya, S.R, S.B. Maharjan, F. Shrestha, W. Guo, S. Liu, W. Immerzeel and B. Shrestha (2015). The glaciers of the Hindu Kush Himalayas: current status and observed changes from the 1980s to 2010. *International Journal of Water Resources Development*, 31, 161-173.

Basnett, S., A.V. Kulkarni, and T. Bolch (2013). The influence of debris cover and glacial lakes on the recession of glaciers in Sikkim Himalaya, India. *Journal of Glaciology*, 59, 1035-1046.

Benn, D.I., T. Bolch, K. Hands, J. Gulley, A. Luckman, L.I. Nicholson, D. Quincey, S. Thompson, R. Toumi and S. Wiseman (2012). Response of debris-covered glaciers in the Mount Everest region to recent warming, and implications for outburst flood hazards. *Earth-Science Reviews*, 114, 156-174.

Benn, D.I., S. Wiseman, and K.A. Hands (2001). Growth and drainage of supraglacial lakes on debris mantled Ngozumpa Glacier, Khumbu Himal, Nepal. *Journal of Glaciology*, 47, 626-638.

Bhatt, M.P., N. Takeuchi and M.F. Acevedo (2016). Chemistry of Supraglacial Ponds in the Debris-Covered Area of Lirung Glacier in Central Nepal Himalayas. *Aquatic Geochemistry*, 22(1), pp.35-64.

Bolch, T., M. Buchroithner, T. Pieczonka and A. Kunert (2008). Planimetric and volumetric glacier changes in the Khumbu Himal, Nepal, since 1962 using Corona, Landsat TM and ASTER data. *Journal of Glaciology*, 54, 592-600.

Bolch, T., A. Kulkarni, A. Kääb, C. Huggel, F. Paul, J.G. Cogley, H. Frey, J.S. Kargel, K. Fujita, M. Scheel and S. Bajracharya (2012). The state and fate of Himalayan glaciers. *Science*, 336, 310-314.

Bonnaventure, P.P. and S.F. Lamoureux (2013). The active layer: A conceptual review of monitoring, modelling techniques and changes in a warming climate. *Progress in Physical Geography*, 37, 352-376.

Bookhagen, B. and D.W. Burbank (2010). Toward a complete Himalayan hydrological budget: Spatiotemporal distribution of snowmelt and rainfall and their impact on river discharge. *Journal of Geophysical Research: Earth Surface*, 115(F3), F03019.

Brun, F., E. Berthier, P. Wagnon, A. Kääb, D. Treichler, H.B. Franz, A.C. McAdam, D.W. Ming, C. Freissinet, P.R. Mahaffy and D.L. Eldridge (2017). A spatially resolved estimate of High Mountain Asia glacier mass balances from 2000 to 2016. *Nature Geoscience*. doi:10.1038/ngeo2999

Brun, F., P. Buri, E.S. Miles, P. Wagnon, J. Steiner, E. Berthier, S. Ragettli, P. Kraaijenbrink, W.W. Immerzeel and F. Pellicciotti (2016). Quantifying volume loss from ice cliffs on debris-covered glaciers using high-resolution terrestrial and aerial photogrammetry. *Journal of Glaciology*, 62, 684-695.

Carenzo, M., F. Pellicciotti, J. Mabillard, T. Reid and B.W. Brock (2016). An enhanced temperature index model for debris-covered glaciers accounting for thickness effect. *Advances in Water Resources*, 94, 457-469.

403 Di Baldassarre, G. and A. Montanari (2009). Uncertainty in river discharge observations: a
404 quantitative analysis. Hydrology and Earth System Sciences, 13(6), 913-921. DOI:
405 10.5194/hess-13-913-2009

406 Evatt, G.W., I.D. Abrahams, M. Heil, C. Mayer, J. Kingslake, S.L. Mithcel, A.C. Flower and
407 C.D. Clark (2015). Glacial melt under a porous debris layer. *Journal of Glaciology*. 61,
408 825-836.

409 Fujita, K. and A. Sakai (2014). Modelling runoff from a Himalayan debris-covered glacier.
410 *Hydrology and Earth System Sciences*, 18, 2679–2694.

411 Gades, A., H. Conway, N. Nereson, N. Naito and T. Kadota. (2000). Radio echo-sounding
412 through supraglacial debris on Lirung and Khumbu Glaciers, Nepal Himalayas. *IAHS*
413 *Publication*, 264, 13-24.

414 Gardelle, J., Y. Arnaud and E. Berthier (2011). Contrasted evolution of glacial lakes along the
415 Hindu Kush Himalaya mountain range between 1990 and 2009. *Global and Planetary*
416 *Change*, 75, 47-55 (2011).

417 Gulley, J. and D.I. Benn (2007). Structural control of englacial drainage systems in Himalayan
418 debris-covered glaciers. *Journal of Glaciology*, 53, 399-412.

419 Gulley, J.D., D.I. Benn, D. Müller and A. Luckman (2009). A cut-and-closure origin for
420 englacial conduits in uncrevassed regions of polythermal glaciers. *Journal of Glaciology*,
421 55, 66-80.

422 Gurnell A.M. (1993). How many reservoirs? An analysis of flow recessions from a glacier basin.
423 *Journal of Glaciology* 39, 132-134.

424 Hannah, D.M., B.P. Smith, A.M. Gurnell and G.R. McGregor (2000). An approach to
425 hydrograph classification. *Hydrological Processes*, 14, 317-338.

426 Herschy, R.W., 1995. Streamflow measurement. CRC Press.

427 Hodgkins, R., R. Cooper, M. Tranter and J. Wadham (2013). Drainage system development in
428 consecutive melt seasons at a polythermal, Arctic glacier, evaluated by flow recession
429 analysis and linear reservoir simulation. *Water Resources Research*, 49, 4230-4243.

430 Hudson, R. and J. Fraser (2005). The mass balance (or dry injection) method. *Streamline*
431 *Watershed Management Bulletin*, 9, 6-12.

432 Immerzeel, W.W. and M.F.P. Bierkens (2012). Asia's water balance. *Nature Geoscience*, 5, 841-
433 842.

434 Immerzeel, W.W., L.P.H. Van Beek and M.F.P. Bierkens (2010) Climate change will affect the
435 Asian water towers. *Science*, 328, 1382–1385.

436 Immerzeel, W.W., L.P.H. Van Beek, M. Konz, A.B. Shrestha and M.F.P. Bierkens (2012).
437 Hydrological response to climate change in a glacierized catchment in the Himalayas.
438 *Climatic Change*, 110, 721-736..

439 Jacobsen, D., A.M. Milner, L.E. Brown and O. Dangles (2012). Biodiversity under threat in
440 glacier-fed river systems. *Nature Climate Change*, 2, 361-364.

441 Jobard, S. and M. Dzikowski (2006). Evolution of glacial flow and drainage during the ablation
442 season. *Journal of Hydrology*, 330, 663-671.

443 Kääb, A., E. Berthier, C. Nuth, J. Gardelle and Y. Arnaud (2012) Contrasting patterns of early
444 twenty-first-century glacier mass change in the Himalayas. *Nature*, 488, 495-498.

445 King, O., D.J. Quincey, J.L. Carrivick and A.V. Rowan (2017). Spatial variability in mass loss of
446 glaciers in the Everest region, central Himalayas, between 2000 and 2015. *The*
447 *Cryosphere*, 11, 407-426.

448 Kirkbride, M.P. (1993). The temporal significance of transitions from melting to calving termini
449 at glaciers in the central Southern Alps of New Zealand. *The Holocene*, 3, 232-240.

450 Lang, H. (1973). Variations in the relation between glacier discharge and meteorological
451 elements. *IAHS Publication*, 95, 85-96.

452 Lutz, A. F., W.W. Immerzeel, A.B. Shrestha and M.F.P. Bierkens (2014). Consistent increase in
453 High Asia's runoff due to increasing glacier melt and precipitation. *Nature Climate*
454 *Change*, 4, 587-592.

455 McCarthy, M., H. Pritchard, I. Willis and E. King (2017). Ground-penetrating radar
456 measurements of debris thickness on Lirung Glacier, Nepal. *Journal of Glaciology*, 63,
457 543-555.

458 Mae, S., H. Wushiki, Y. Ageta and K. Higuchi (1975). Thermal drilling and temperature
459 measurements in Khumbu Glacier, Nepal Himalayas. *Seppyo*, 37, 161-169.

460 Mertes, J.R., S.S. Thompson, A.D. Booth, J.D. Gulley and D.I. Benn (2017). A conceptual
461 model of supra-glacial lake formation on debris-covered glaciers based on GPR facies
462 analysis. *Earth Surface Processes and Landforms*, 42, 903-914.

463 Miles, E.S., F. Pellicciotti, I.C. Willis, J.F. Steiner, P. Buri and N.S. Arnold (2016). Refined
464 energy-balance modelling of a supraglacial pond, Langtang Khola, Nepal. *Annals of*
465 *Glaciology*, 57, 29-40.

466 Miles, E.S., I.C. Willis, N.S. Arnold, J. Steiner and F. Pellicciotti (2017a). Spatial, seasonal and
467 interannual variability of supraglacial ponds in the Langtang Valley of Nepal, 1999–
468 2013. *Journal of Glaciology*, 63, 88-105.

469 Miles, E.S., J. Steiner, I. Willis, P. Buri, W.W. Immerzeel, A. Chesnokova, and F. Pellicciotti
470 (2017b). Pond Dynamics and Supraglacial-Englacial Connectivity on Debris-Covered
471 Lirung Glacier, Nepal. *Frontiers in Earth Science*, 5, 69.

472 Montaldo, N., M. Mancini and R. Rosso (2004). Flood hydrograph attenuation induced by a
473 reservoir system: analysis with a distributed rainfall-runoff model. *Hydrological*
474 *Processes*, 18, 545-563.

475 Muir, D.L., M. Hayashi and A.F. McClymont (2011). Hydrological storage and transmission
476 characteristics of an alpine talus. *Hydrological Processes*, 25, 2954-2966.

477 Narama, C., M. Daiyrov, T. Tadono, M. Yamamoto, A. Kääb, R. Morita and J. Ukita (2017).
478 Seasonal drainage of supraglacial lakes on debris-covered glaciers in the Tien Shan
479 Mountains, Central Asia. *Geomorphology*, 286, 133-142.

Nuimura, T., K. Fujita, K. Fukui, K. Asahi, R. Aryal and Y. Ageta (2011). Temporal changes in elevation of the debris-covered ablation area of Khumbu Glacier in the Nepal Himalaya since 1978. *Arctic, Antarctic, and Alpine Research*, 43, 246-255.

Østrem, G. (1959). Ice melting under a thin layer of moraine, and the existence of ice cores in moraine ridges. *Geografiska Annaler*, 41, 228-230.

Parriaux, A., and G.F. Nicoud (1990). Hydrological behaviour of glacial deposits in mountainous areas. *IAHS Publication* 190, 291-312.

Pritchard, H.D., 2017. Asia's glaciers are a regionally important buffer against drought. *Nature*, 545(7653), 169-174.

Quincey, D.J., S.D. Richardson, A. Luckman, R.M. Lucas, J.M. Reynolds, M.J. Hambrey and N.F. Glasser (2007). Early recognition of glacial lake hazards in the Himalaya using remote sensing datasets. *Global and Planetary Change*, 56, 137-152.

Ragettli, S., F. Pellicciotti, W.W. Immerzeel, E.S. Miles, L. Petersen, M. Heynen, J.M. Shea, D. Stumm, S. Joshi and A. Shrestha (2015). Unraveling the hydrology of a Himalayan catchment through integration of high resolution in situ data and remote sensing with an advanced simulation model. *Advances in Water Resources*, 78, 94-111.

Rantz, S.E., and others (1982). Measurement and computation of streamflow: Volume 2. Computation of discharge. USGS Water Supply Paper 2175. USGPO, 285-631.

Reynolds, J.M. (2000). On the formation of supraglacial lakes on debris-covered glaciers. *IAHS Publication*, 264, 153-164.

Richards, K., M. Sharp, N. Arnold, A. Gurnell, M. Clark, M. Tranter, P. Nienow, G. Brown, I. Willis and W. Lawson (1996). An integrated approach to modelling hydrology and water quality in glacierized catchments. *Hydrological Processes*, 10, 479-508.

Rowan, A.V., D.L. Egholm, D.J. Quincey and N.F. Glasser (2015). Modelling the feedbacks between mass balance, ice flow and debris transport to predict the response to climate change of debris-covered glaciers in the Himalaya, *Earth and Planetary Science Letters*, 430, 427-438.

Sakai, A., K. Fujita, T. Aoki, K. Asahi, and M. Nakawo (1997). Water discharge from the Lirung Glacier in Langtang Valley, Nepal Himalayas, 1996. Bulletin of Glacier Research 15, 79-83.

Sakai, A., M. Nakawo and K. Fujita (2002). Distribution characteristics and energy balance of ice cliffs on debris-covered glaciers, Nepal Himalaya. *Arctic, Antarctic, and Alpine Research*, 34, 12-19.

Sakai, A., N. Takeuchi, K. Fujita and M. Nakawo (2000). Role of supraglacial ponds in the ablation process of a debris-covered glacier in the Nepal Himalayas. *IAHS Publication*, 264, 119-132.

Salerno, F., M. Rogora, R. Balestrini, A. Lami, G.A. Tartari, S. Thakuri, D. Godone, M. Freppaz and G. Tartari (2016). Glacier melting increases the solute concentrations of Himalayan glacial lakes. *Environmental Science & Technology*, 50, 9150-9160.

519 Salerno, F., S. Thakuri, G. Tartari, T. Nuimura, S. Sunako, A. Sakai, K. Fujita. 2017. Debris-
520 covered glacier anomaly? Morphological factors controlling changes in the mass balance,
521 surface area, terminus position, and snow line altitude of Himalayan glaciers. *Earth and*
522 *Planetary Science Letters*, 471, 19-31.

523 Scherler, D., B. Bookhagen and M.R. Strecker (2011). Spatially variable response of Himalayan
524 glaciers to climate change affected by debris cover. *Nature Geoscience*, 4, 156-159.

525 Schmid, M.O., P. Baral, S. Gruber, S. Shahi, T. Shrestha, D. Stumm and P. Wester (2015).
526 Assessment of permafrost distribution maps in the Hindu Kush Himalayan region using
527 rock glaciers mapped in Google Earth. *The Cryosphere*, 9, 2089-2099.

528 Shea, J.M., W.W. Immerzeel, P. Wagnon, C. Vincent and S. Bajracharya (2015a). Modelling
529 glacier change in the Everest region, Nepal Himalaya. *The Cryosphere*, 9, 1105-1128.

530 Shea J.M., P. Wagnon, W.W. Immerzeel, R. Biron, F. Brun and F. Pellicciotti. (2015b). A
531 comparative high-altitude meteorological analysis from three catchments in the Nepalese
532 Himalaya, *International Journal of Water Resources Development*, 31, 174-200.

533 Sherpa, S.F., P. Wagnon, F. Brun, E. Berthier, C. Vincent, Y. Lejeune, Y. Arnaud, R.B.
534 Kayastha and A. Sinisolo (2017). Contrasted surface mass balances of debris-free
535 glaciers observed between the southern and the inner parts of the Everest region (2007–
536 15). *Journal of Glaciology*, XX, 1-15. doi: 10.1017/jog.2017.30

537 Soncini, A., D. Bocchiola, G. Confortola, U. Minora, E. Vuillermoz, F. Salerno, G. Viviano, D.
538 Shrestha, A. Senese, C. Smiraglia, and G. Diolaiuti (2016). Future hydrological regimes
539 and glacier cover in the Everest region: The case study of the upper Dudh Koshi basin.
540 *Science of the Total Environment*, 565, 1084-1101. doi: 10.1016/j.scitotenv.2016.05.138

541 Steiner, J.F. and F. Pellicciotti (2016). Variability of air temperature over a debris-covered
542 glacier in the Nepalese Himalaya. *Annals of Glaciology*, 57, 295-307.

543 Swift, D.A., P.W. Nienow, T.B. Hoey and D.W. Mair (2005). Seasonal evolution of runoff from
544 Haut Glacier d'Arolla, Switzerland and implications for glacial geomorphic processes.
545 *Journal of Hydrology*, 309,133-148.

546 Takeuchi, N., A. Sakai, K. Shiro, K. Fujita and N. Masayoshi (2012). Variation in suspended
547 sediment concentration of supraglacial lakes on debris-covered area of the Lirung Glacier
548 in the Nepal Himalayas. *Global Environmental Reseach*, 16, 95-104.

549 Thakuri, S., F. Salerno, C. Smiraglia, T. Bolch, C. D'Agata, G. Viviano and G. Tartari (2014).
550 Tracing glacier changes since the 1960s on the south slope of Mt. Everest (central
551 Southern Himalaya) using optical satellite imagery. *The Cryosphere*, 8, 1297-1315.

552 Thayyen, R.J., J.T. Gergan and D.P. Dobhal (2005). Monsoonal control on glacier discharge and
553 hydrograph characteristics, a case study of Dokriani Glacier, Garhwal Himalaya, India.
554 *Journal of Hydrology*, 306, 37-49.

555 Thompson, S., D.I. Benn, J. Mertes and A. Luckman (2016). Stagnation and mass loss on a
556 Himalayan debris-covered glacier: processes, patterns and rates. *Journal of Glaciology*,
557 62, 67-485.

Verbunt, M., J. Gurtz, K. Jasper, H. Lang, P. Warmerdam, and M. Zappa (2003). The hydrological role of snow and glaciers in alpine river basins and their distributed modeling. *Journal of Hydrology*, 282(1), 36-55.

Vincent, C., P. Wagnon, J.M.. Shea, W.W. Immerzeel, P. Kraaijenbrink, D. Shrestha, A. Soruco, Y. Arnaud, F. Brun, E. Berthier, S.F. Sherpa (2016). Reduced melt on debris-covered glaciers: investigations from Changri Nup Glacier, Nepal. *The Cryosphere*, 10, 1845-1858.

Watson, S. C., D.J. Quincey, J.L. Carrivick and M.W. Smith (2016). The dynamics of supraglacial water storage in the Everest region, central Himalaya. *Global and Planetary Change*, 142, 14-27.

Watson, C.S., D.J. Quincey, J.L. Carrivick, M.W. Smith, A.V. Rowan and R. Richardson (2017a). Heterogeneous water storage and thermal regime of supraglacial ponds on debris-covered glaciers. *Earth Surface Processes and Landforms* (early view) doi: 10.1002/esp.4236.

Watson, C.S., D.J. Quincey, J.L. Carrivick and M.W. Smith (2017b). Ice cliff dynamics in the Everest region of the Central Himalaya. *Geomorphology*, 278, 238-251.

Wessels, R.L., J.S. Kargel and H.H. Kieffer (2002). ASTER measurement of supraglacial lakes in the Mount Everest region of the Himalaya. *Annals of Glaciology*, 34, 399-40.

Woo, M.K. and P. Steer (1983). Slope hydrology as influenced by thawing of the active layer, Resolute, NWT. *Canadian Journal of Earth Sciences*, 20, 978-986.

Woo, M.K. and Z. Xia (1995). Suprapermafrost groundwater seepage in gravelly terrain, Resolute, NWT, Canada. *Permafrost and Periglacial Processes*, 6(1), 57-72.

Xu, J., R.E. Grumbine, A. Shrestha, M. Eriksson, X. Yang, Y. Wang and A. Wilkes (2009). The melting Himalayas: cascading effects of climate change on water, biodiversity, and livelihoods. *Conservation Biology*, 23, 520-530.

Figure 1.

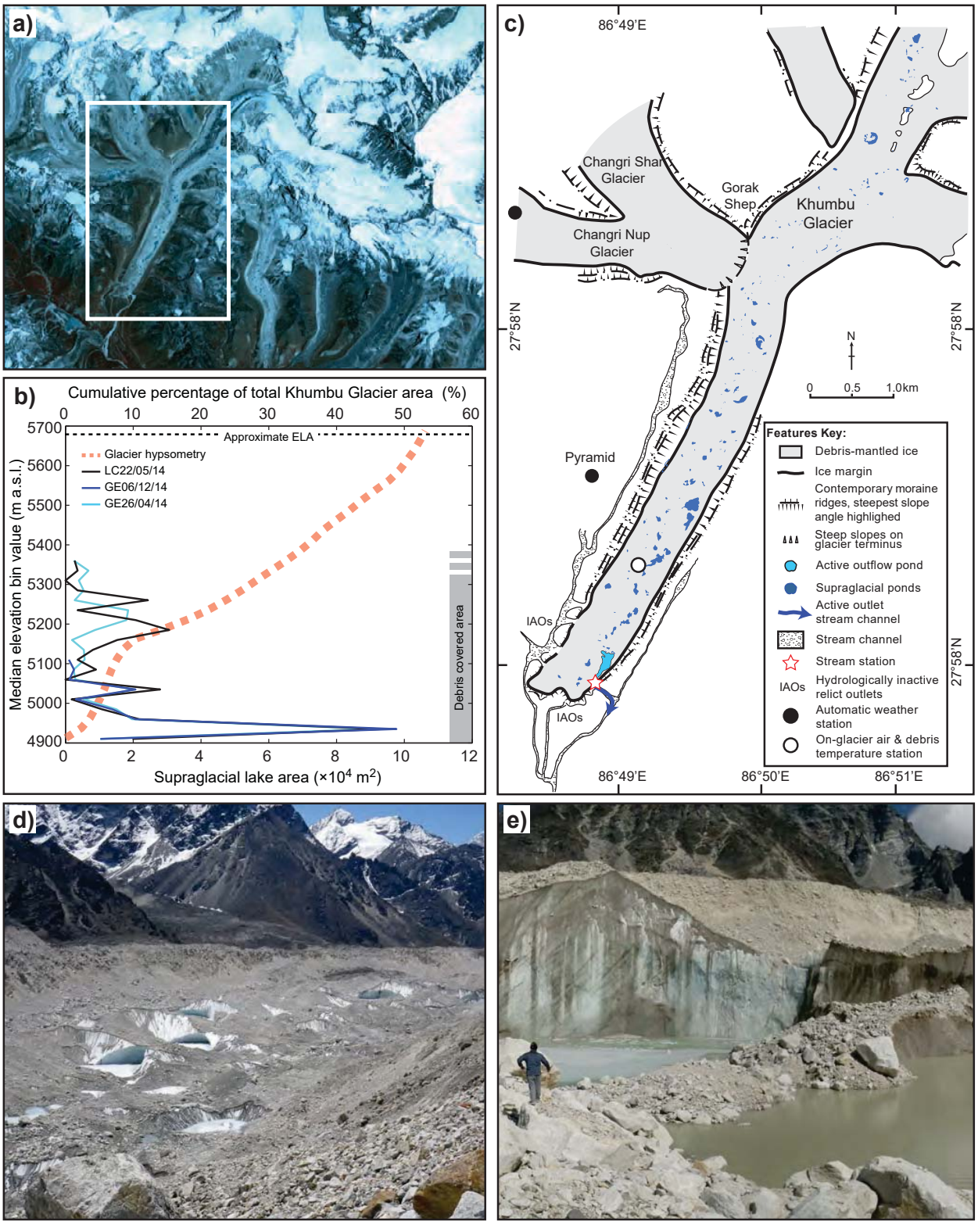
a)
b)
Cumulative percentage of total Khumbu Glacier area (%)
0
10
20
30
40
50
60
Approximate ELA
Glacier hypsometry
LC22/05/14
GE06/12/14
GE26/04/14
Debris covered area
Median elevation bin value (m a.s.l.)
5700
5600
5500
5400
5300
5200
5100
5000
4900
0
2
4
6
8
10
12
Supraglacial lake area (×10^4 m^2)
c)
86°49'E
Changri Shar Glacier
Gorak Shep
Khumbu Glacier
Changri Nup Glacier
27°58'N
N
0
0.5
1.0km
Pyramid
IAOs
IAOs
Features Key:
Debris-mantled ice
Ice margin
Contemporary moraine ridges, steepest slope angle highlighted
Steep slopes on glacier terminus
Active outflow pond
Supraglacial ponds
Active outlet stream channel
Stream channel
Stream station
IAOs
Hydrologically inactive relict outlets
Automatic weather station
On-glacier air & debris temperature station
86°49'E
86°50'E
86°51'E
d)
e)

Figure 2.

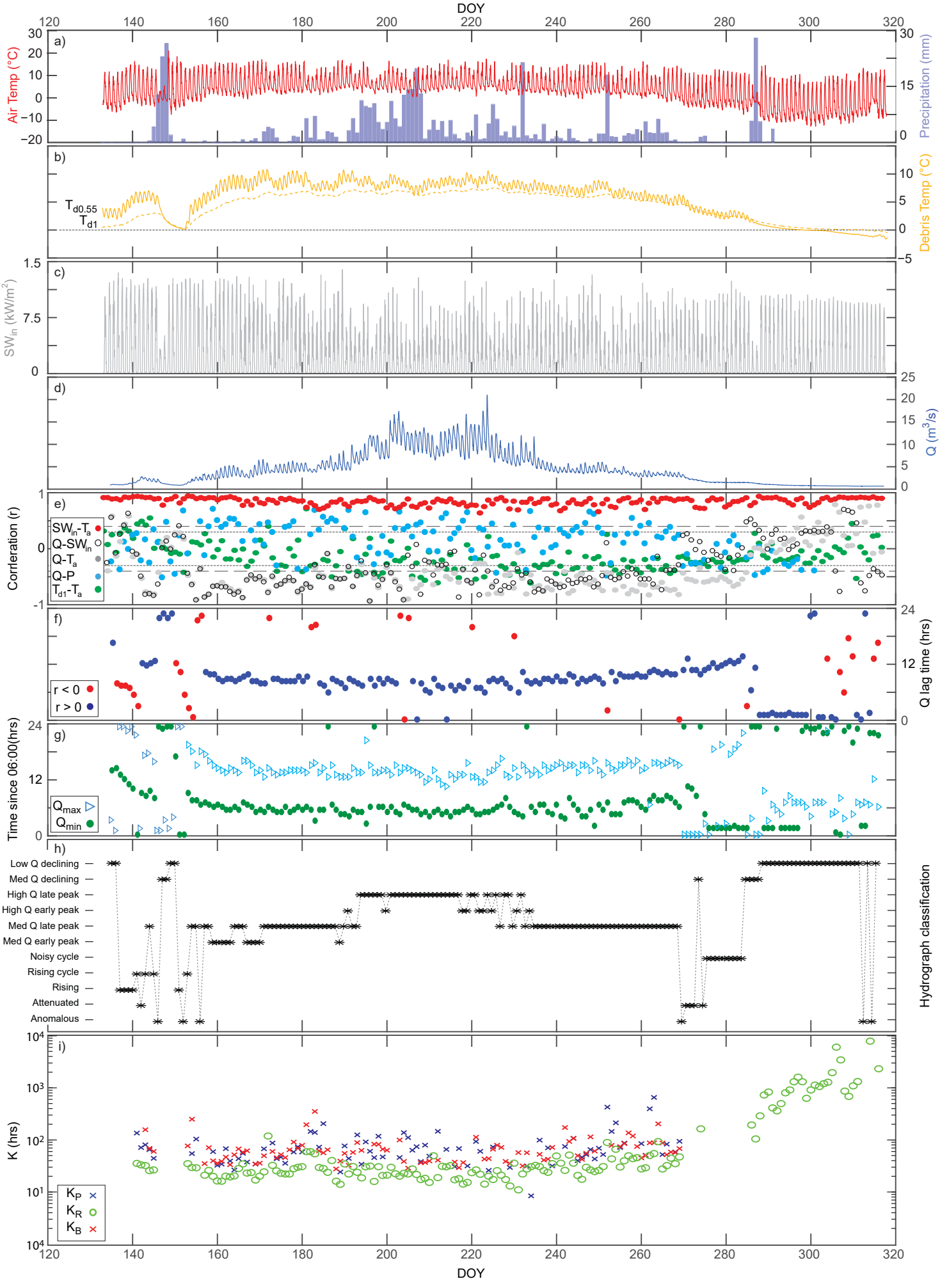
DOY
a)
Air Temp (°C)
Precipitation (mm)
b)
$T_{d0.55}$
T_{d1}
Debris Temp (°C)
c)
SW_{in} (kW/m^2)
d)
Q (m^3/s)
e)
Correlation (r)
SW_{in}-T_a
Q-SW_{in}
Q-T_a
Q-P
T_{d1}-T_a
f)
r < 0
r > 0
Q lag time (hrs)
g)
Time since 06:00(hrs)
Q_{max}
Q_{min}
h)
Low Q declining
Med Q declining
High Q late peak
High Q early peak
Med Q late peak
Med Q early peak
Noisy cycle
Rising cycle
Rising
Attenuated
Anomalous
Hydrograph classification
i)
K (hrs)
K_P
K_R
K_B
DOY

Figure 3.

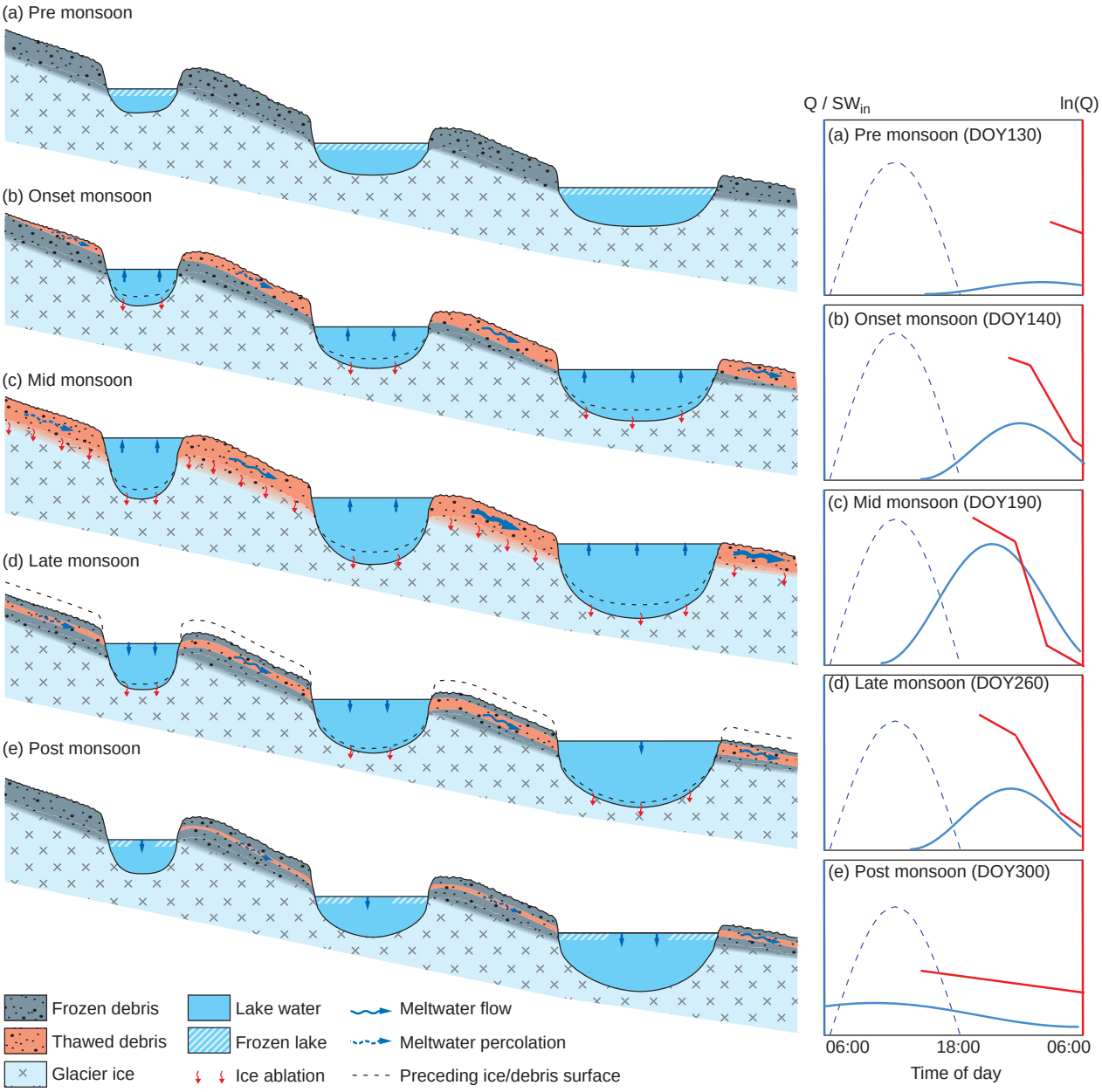
(a) Pre monsoon
(b) Onset monsoon
(c) Mid monsoon
(d) Late monsoon
(e) Post monsoon
Frozen debris
Thawed debris
Glacier ice
Lake water
Frozen lake
Ice ablation
Meltwater flow
Meltwater percolation
Preceding ice/debris surface
Q / SWin
ln(Q)
(a) Pre monsoon (DOY130)
(b) Onset monsoon (DOY140)
(c) Mid monsoon (DOY190)
(d) Late monsoon (DOY260)
(e) Post monsoon (DOY300)
06:00
18:00
06:00
Time of day